PMM Science Team Meeting – San Diego 16-20 Orcober 2017

Use of coincident radar and radiometer observations from GPM and CloudSat for global spaceborne snowfall observation assessment

Giulia Panegrossi, Daniele Casella, Stefano Dietrich, Anna Cinzia Marra, Jean-François Rysman, Paolo Sanò *CNR-ISAC, Rome, Italy*
Mark S. Kulie, *Michigan Technological University, MI, USA* Benjamin T. Johnson, *UARC/JCSDA@NOAA College Park, MD, USA*

Objectives

Main goal: To prepare and exploit datasets from coincident overpasses of spaceborne precipitation radars [GPM Dual-frequency Precipitation Radar (DPR) and CloudSat Cloud Profiling Radar (CPR)] and of CloudSat CPR with PMW radiometers in the GPM constellation (AMSU/MHS, AMSR-E, ATMS and GMI) towards the refinement and development of precipitation retrieval techniques (**snowfall).**

1. **GPM-DPR vs. CloudSat CPR**: comparison of snowfall detection capabilities, definition of limitations and potentials of DPR with respect to CPR in the detection of snowfall, assessment of global snowfall mass estimate by DPR vs. CPR;
2. **Analysis of GMI/CPR coincidence datasets** to define the limitations and capabilities of the Global Precipitation Measurement (GPM) mission Microwave Imager (GMI) to observe snowfall (in particular at high latitudes) in relation to environmental characteristics (i.e., background surface and integrated water vapor content)

DPR vs. CloudSat CPR *(Casella et al., 2017)*

39,975 coincident DPR-CPR snowfall observations from 2B-CSATGPM product for the period March 2014 to May 2015. Selected coincidences within 5 minutes and 2.5 km. Ancillary data and products have been also included

Case Study: Widespread frontal snowfall Eastern Russia/Sea of Okhotsk 30 April 2014

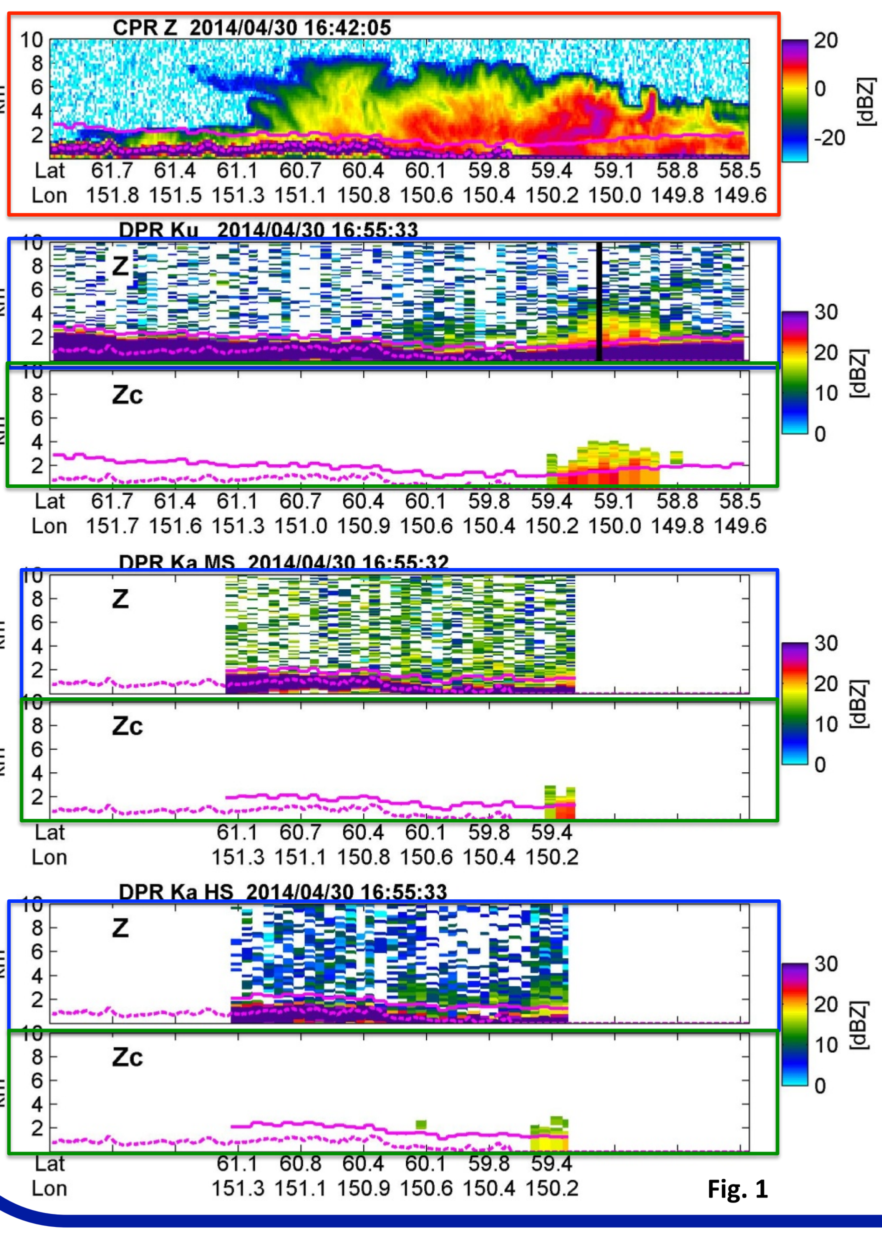

Fig. 1

Figure 1: Comparison of DPR and CPR reflectivity for one case study in the DPR/CPR coincidence dataset

CPR:
- Typical maximum CPR Z: 10-15 dBZ
- maximum cloud top heights at ~5-8 km
- shallower cloud structures with cloud top heights less than ~2 km

DPR Measured Reflectivity (Z)
- Ku and Ka-HS uncorrected Z show some structure below ~4 km in the deeper snowfall segment
- most of the event north of 60° latitude and at higher altitudes is missed
- significant random noise around 12 dBZ (Ku and Ka HS) or 16 dBZ (Ka MS)
- Side lobe clutter signal in the Ku

DPR Corrected Reflectivity (Zc) (2A-DPR)
- Complete suppression of random noise and side lobe clutter
- Attenuation correction below the free-clutter level
- Part of the weak signal related to snowfall is also eliminated

	2B-DPR CMB Ku	2B-DPR CMB Ka MS	2A-DPR Ku	2A-DPR Ka MS	2A-DPR Ka HS
ME *[mm h⁻¹]*	**-0.320** *-0.375*	**-0.261** *-0.315*	**-0.099** *-0.120*	**-0.075** *-0.075*	**-0.519** *-0.615*
RMSE *[mm h⁻¹]*	**0.611** *0.701*	**0.650** *0.775*	**0.633** *0.712*	**0.682** *0.786*	**0.819** *0.947*
ARMSE *[mm h⁻¹]*	**0.520** *0.593*	**0.595** *0.708*	**0.625** *0.702*	**0.678** *0.782*	**0.634** *0.720*

Table 1: Continuous statistics (hits only) for DPR products **Solid and mixed precipitation** (melted fraction <=0.1); *Solid-only precipitation*

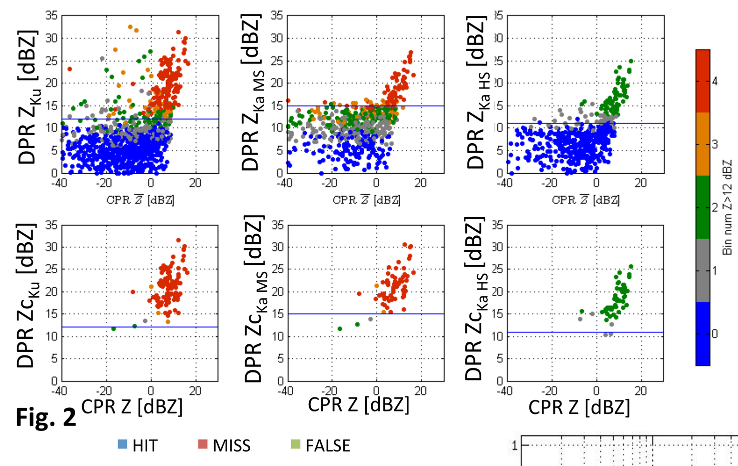

Fig. 2

Fig.2: Mean reflectivity from DPR (**measured top and corrected bottom**) compared to the mean CPR reflectivity in a layer 500 m thick above the DPR FCBH. Color scale: number of pixels in the 500 m layer with DPR reflectivity higher than 12 dBZ. In DPR Zc observations with relatively weak echoes close to the sensitivity threshold are eliminated.

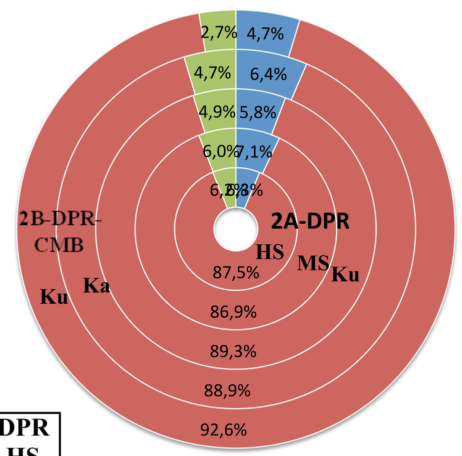

***Fig. 3:* Very high % of MISS.** DPR-Ka Hs shows best performance. ***False Alarms** mostly due to inconsistencies in the precipitation phase between DPR and CPR products (FCBH and in the FLH)*

CPR 2C-SNOW-PROFILE surface snowfall rate is used at reference.

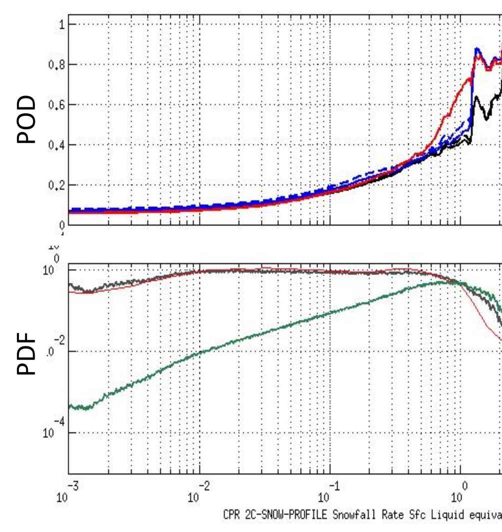

POD for DPR products (V4) for a varying minimum threshold of CPR SR;
PDF by occurrence (PDFc) and by volume (PDFv) from 2 years (2014-2015) of global CPR snowfall observations (in red the PDFc in the CPR-DPR coincidence dataset).

Proposed algorithm to increase DPR snowfall detection capabilities

1. Ka and Ku coherence: -0.5 < DFR < 0.5 (DFR=dBZ_{Ku}-dBZ_{Ka})
2. Cloud structure continuity: Z_{Ku} > 8 dBZ (for at least 3 bins above FCBH);
3. $\bar{Z}_{Ka} > 10 dBZ$ (Z mean in the 500 m layer above FCBH)

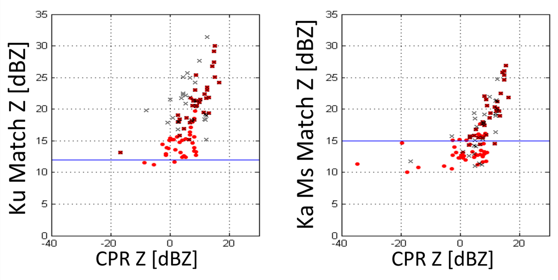

Fig. 4: Red dots: snowfall pixels selected by the new algorithm **+** : snowfall pixels selected by 2A-DPR

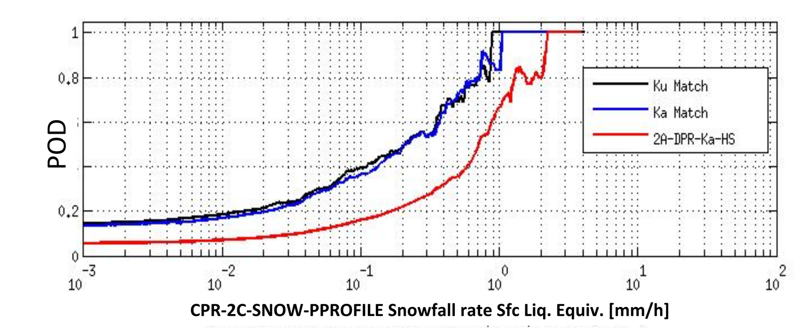

Fig. 5: POD for New algorithm compared to DPR Ka HS

Estimate of snowfall mass detected by DPR vs. CPR 2C-SNOW

DPR Algorithms V4	2B-DPR-CMB Ku	2A-DPR Ku	2B-DPR-CMB Ka MS	2A-DPR Ka MS	2A-DPR Ka HS
	29.9%	29.1%	34.3%	32.8%	32.4%
NEW algorithm	Ku Match 59.0%		Ka Match 54.2%		

GMI vs. CloudSat *(Panegrossi et al., 2017)*

48194 GMI-CPR snowfall observations from 2B-CSATGPM product (available at ftp://arthurhou.pps.eosdis.nasa.gov, courtesy of Dr. J. Turk), for the period March 2014 to May 2016. Ancillary data and CPR/CALIPSO cloud products have been also included

Case Study: Widespread frontal snowfall Eastern Russia/Sea of Okhotsk 30 April 2014

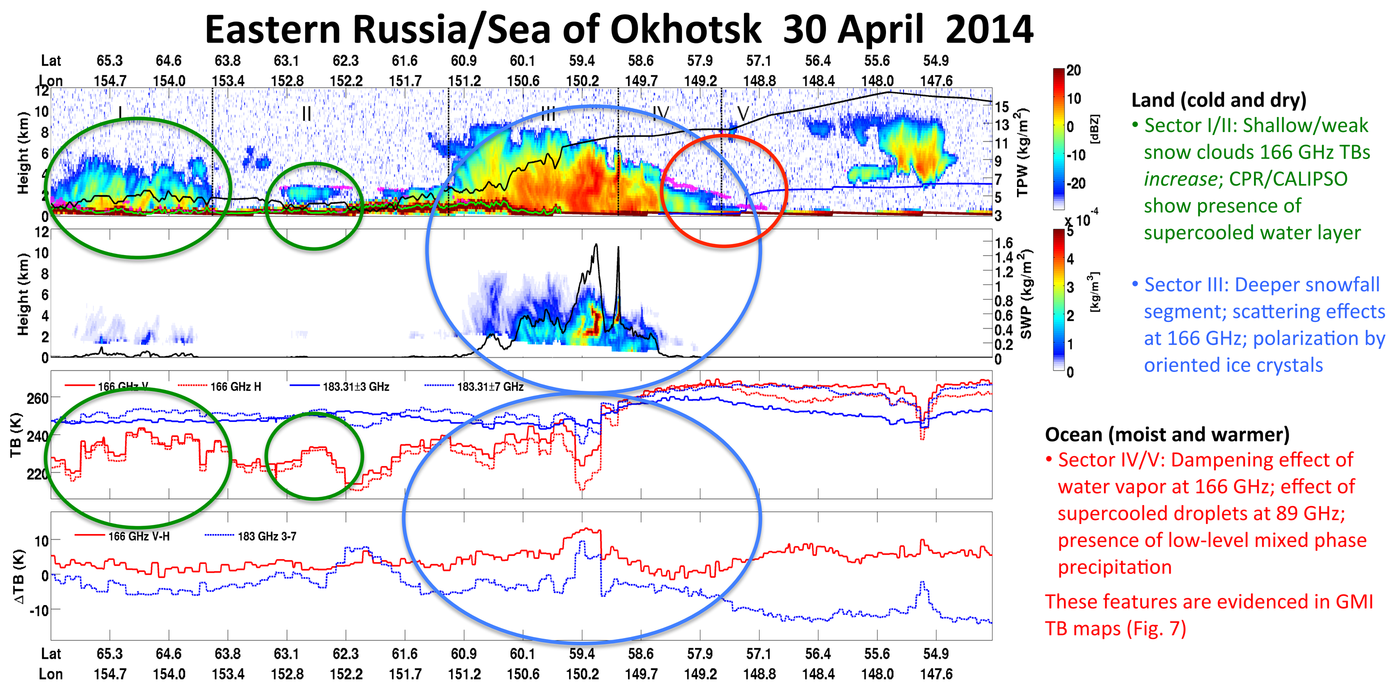

Fig. 6 From top to bottom. First panel CPR reflectivity (colorbar, in dBZ), freezing level height (blue curve), and total precipitable water (TPW) (black curve), along the CloudSat track. Cloud layers where the DARDAR product identifies supercooled droplets are shown in magenta. Second panel 2C-SNOW snow water content (colorbar, in kg m⁻³) and snow water path (SWP) (black curve). Third panel: GMI TBs closest to each CPR pixel along the CloudSat track at 166 GHz (V and H polarization, in red), 183.3±3 GHz and 183.3±7 GHz (in blue). Bottom panel shows GMI TB difference (ΔTB) at 166 GHz (V-H, in red), and for the two 183.3 GHz channels (in blue). In the top panel, vertical lines delineate different Sectors (I to V) identifying different snowfall and environmental conditions.

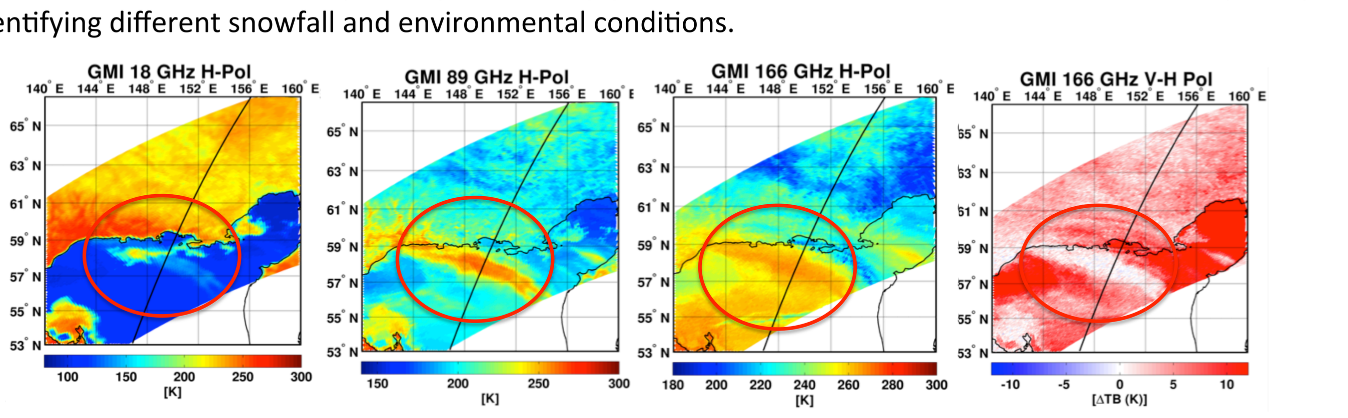

Fig. 7: Maps of GMI TBs (H-pol) at 10 GHz, 18.7 GHz, 89 GHz (H-pol), and 166 GHz (H-pol) for case study shown in Fig. 6 (back lines show CPR track crossing GMI swath).

Effect of supercooled droplets on TBs and ΔTB at 166 GHz

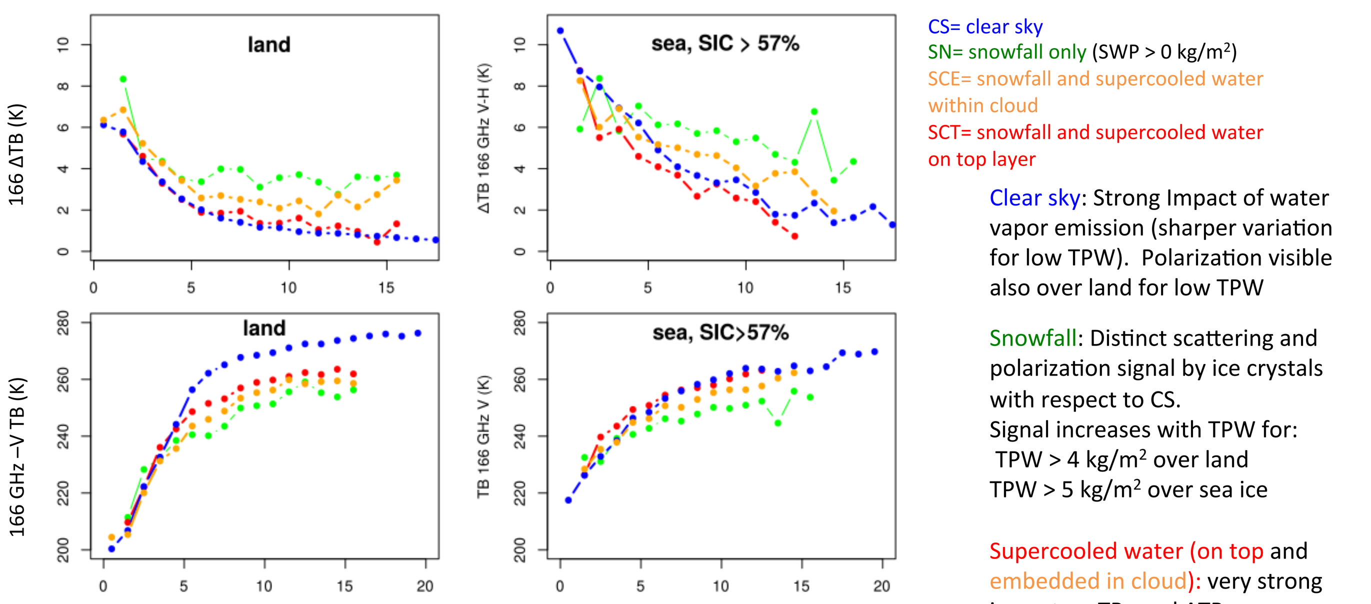

Fig. 8: Median TB and ΔTB values (computed for 21 TPW bins) vs. TPW; results are shown for land (88% frozen) and sea ice (NOAA SNIDC product from AMSR2). Cloud classification is based on CloudSat CPR 2C-SNOW and CPR/CALIPSO DARDAR products

New snowfall detection algorithm based on GMI/CPR coincidence dataset

All-sky frozen surface Classification scheme for GMI

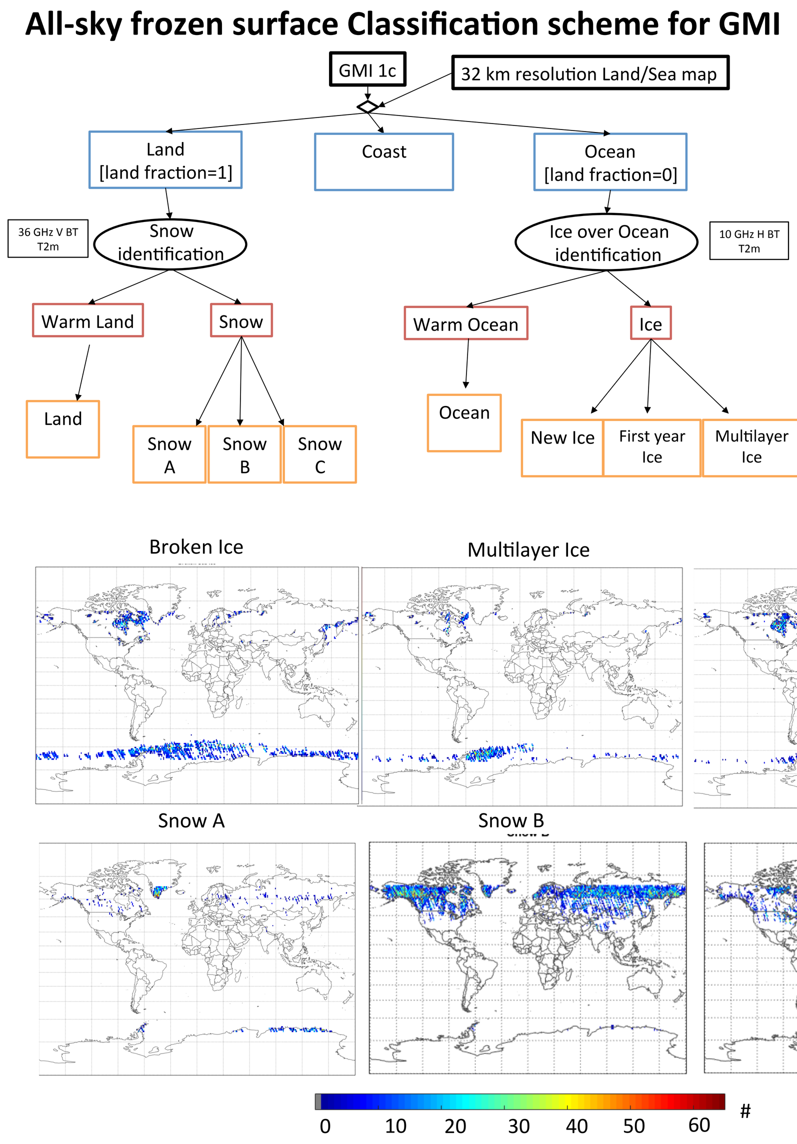

Input: T2m and 10, 23.8, 18.7, 36.5 GHz TBs (pseudo emissivity);
Discriminant functions and k-mean classification.
Sea ice classification is based on based on Hewison and English (1999) (different trends of the emissivity with changing frequency for different types of ice).

Fig. 9: Frozen surface classification scheme for GMI and preliminary results. Ice over ocean: POD= 0.86 FAR 0.03 (vs. Sfc type 2C-PRECIP-COLUMN); snow cover POD=0.90 FAR 0.12 (vs. ERA-I snow depth).

166 ΔTB vs. TPW & Snow Water Path

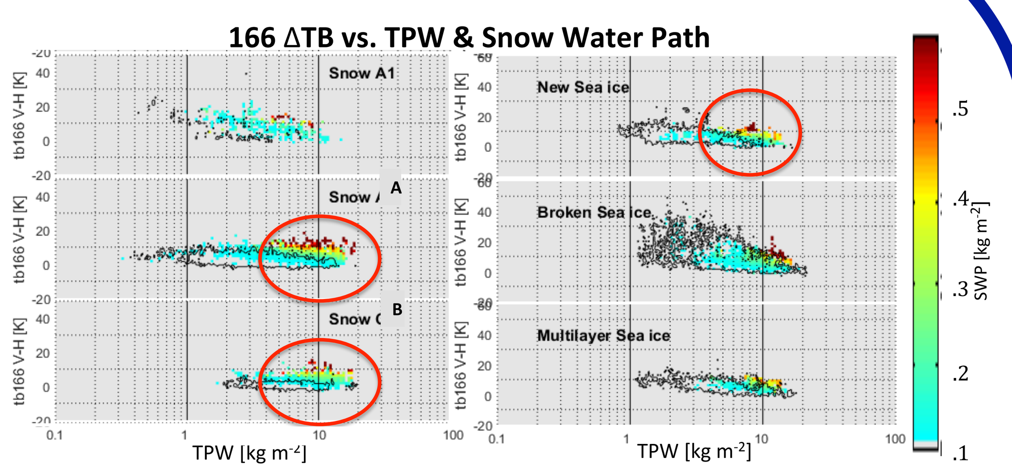

Fig. 10: Scatterplots showing the 166 ΔTB vs. TPW for all the points in the GMI/CPR coincident dataset and for the frozen surface classes. Color scale indicates CPR 2C-SNOW SWP. The black contour delineates the manifold for points in the dataset associated to clear sky (i.e., no cloud according to the 2C-CLASS product) (results for 183 ΔTB show sensitivity to snowfall over ocean.

166 ΔTB vs. TPW & Snowfall Probability

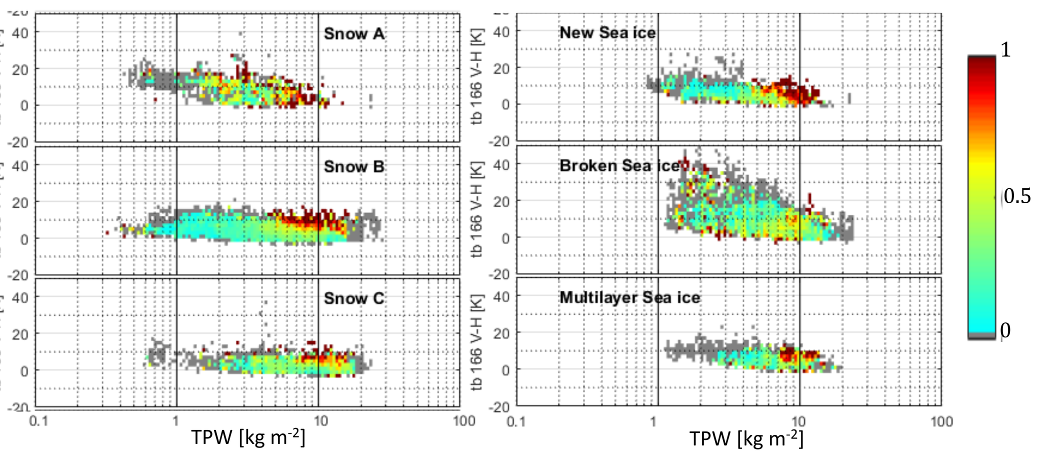

Fig. 11: Scatterplots showing snowfall probability (color scale) for all ΔTB166/TPW 2-D bins in the GMI/CPR coincident dataset and for the frozen surface classes. For each surface type, for a given combination (bin) of ΔTB166/TPW snowfall probability is calculated as Ns/(Ns+N0) where Ns is number of occurrences of CPR 2C-SNOW surface snowfall rate > 0 mm/h, N0 occurrences without CPR 2C-SNOW surface snowfall.

- Over Snow B, Snow C and New Sea Ice, snowfall probability is larger when TPW > 5 kg/m² (confirming results of Fig. 8)
- For Snow B and Snow C the largest probabilities are associated with larger 166 ΔTB. For New Sea Ice, large snowfall probabilities are associated with 166 ΔTB < 10 K. Over Multilayer Sea Ice, larger probabilities occur for TPW > 8 kg/m². In these cases, higher probabilities are associated with higher ΔTB166 (around 10 K).
- Very light snowfall is associated to Snow A;
- Over Broken Ice (and over ocean) 166 ΔTB is not very effective because of the high polarization signal due to the surface.

Similar analysis has been carried out for the 183 GHz channels (183 ΔTB) showing good sensitivity to snowfall over Broken Ice, and over Ocean, and lower sensitivity then 166 ΔTB over snow cover. The combined use of 183ΔTB and 166ΔTB can be very effective for snowfall detection.

Snowfall detection scheme description and preliminary results

1) Preliminary probability of snowfall Ns/(Ns+N0) is based on a 3-D look-up table based on environmental variables (Sims and Liu, 2015]:
   TPW (50 bins, linear scale)
   T2m (50 bins, log scale)
   Lapse rate 2-500 m (20 bins, linear scale)
   The full CPR database (2006-2011) (day and night) has been used to build the 3-D look-up table.
2) If preliminary probability of snowfall based on 1) is higher than 10% the probability of snowfall is computed based on a 4-D look-up table built upon:
   Surface type
   TPW
   ΔTb 166 GHz V-H
   ΔTb 183±3 -183±7 GHz
   The GMI/CPR coincident observation dataset has been used to build the 4-D look-up table.

	Ocean	New Sea ice	Broken Sea ice	Multilayer Sea ice	Land	Snow A	Snow B	Snow C	Coast
# of snow pixels/ total pixels	1919/ 23664	120/ 336	454/ 1123	58/ 180	73/ 13488	32/ 62	85/ 353	111/ 291	72/ 2195
POD	0.80	0.60	0.83	0.72	0.19	0.31	0.54	0.74	0.74
FAR	0.40	0.35	0.47	0.54	0.74	0.09	0.36	0.49	0.37
HSS	0.65	0.43	0.31	0.28	0.22	0.27	0.47	0.28	0.67

Table 2: **Verification with indipendent GMI/CPR dataset June-Dec. 2016.** For each surface type the value of the probability of snowfall that maximizes the HSS in the training dataset is selected as the value to evaluate the snowfall detection capabilities. "Truth" is CPR 2C-PRECIP Precipitation Flag: Snow Possible or Certain, or Mixed Precip. (liquid fraction < 01.).

Contact: g.panegrossi@isac.cnr.it)

References

Casella, et al., Evaluation of the GPM-DPR snowfall detection capability: Comparison with CloudSat-CPR, Atmospheric Research, 197, 64-75, doi :10.1016/j.atmosres.2017.06.018, 2017
Panegrossi et al., CloudSat-based assessment of GPM Microwave Imager snowfall detection capabilities, 2017, *Remote Sensing*, Submitted
Sims E. and G. Liu, 2015, *https://doi.org/10.1175/JHM-D-14-0211.1*
Hewison, T.J., and S.J. English 1999, doi:10.1109/36.774700.

Acknowledgements

This research was carried out within the **EUMETSAT H-SAF Federated Activity FA_15_01** with the NASA PMM Science Team: ***Cooperation on the use of combined spaceborne active and passive MW observations for precipitation retrieval***. It was supported by the EUMETSAT "Satellite Application Facility on Support to Operational Hydrology and Water Management" (H-SAF) and partly by the EarthH2Observe project funded under the EU DG Research 7th Framework Programme (FP7). The authors are very grateful to *Dr. Joe Turk (NASA JPL)* and NASA PPS for providing the 2B-CSATGPM database which is at the base of this study.